

ATLAS COLLABORATION

Search for supersymmetric neutral Higgs h in the decay $\rightarrow \mu^+\mu^-$ in ATLAS detector at LHC

Simonetta Gentile Mercedes Paniccia

Paolo Violini

Dipartimento di Fisica, Università La Sapienza, Sez. I.N.F.N., Roma.

ATL-PHYS-2003-013
05 June 2003



Abstract

Results are presented on the possibility of MSSM h discovery in region of high $\tan\beta$, larger than 15, and mass close to 100 GeV in the channel $h \rightarrow \mu^+\mu^-$, accompanied by two b-jets. This region not completely covered from neither LEP neither Tevatron data constitutes a potential test for the MSSM Higgs discovery. In this note the use of an experimental technique to evaluate the most copious background, $Z \rightarrow \mu^+\mu^-$, with a different approach from a previous one [1], is proposed with promising results.

1 Introduction

The Minimal Supersymmetric Standard Model (MSSM) is the most investigated extension of the Standard Model (SM).

The theory requires two Higgs doublets. This gives rise to five Higgs bosons: a charged scalar pair, two neutral CP-even, the lightest to which is called h and a neutral CP-odd, A [2–4]. The discovery of any one of these particles is crucial to prove such models. This is a key point in the physics program of future accelerators and in particular of LHC.

After the conclusion of the LEP program, in the year 2000, mass limits on the Standard Model Higgs boson H [5], on existence of charged [6], H^\pm , and neutral Higgs bosons [7], h and A , are established in most of representative cases of the model parameters.

Then it is a natural consequence, that is the motivation of this study, to explore the potentiality for a discovery of the neutral Higgs MSSM bosons in the region not excluded by the LEP data, exploiting the performances of the ATLAS detector.

The non excluded region, where the h mass is close to m_Z , the mass of the Z boson, constitutes a challenging test for the detector performance and the analysis method to disentangle the signal from the background.

In the following sections are discussed: the motivation of this study in the MSSM framework, the present experimental situation, the discovery potential of others Higgs MSSM channels, the description of the Monte Carlo generator and the software tools used, results on potential discovery or in negative case of exclusion and conclusions.

2 Minimal Supersymmetric Standard Model

In this paragraph the fundamental points of the model, useful for the following discussion are summarized, referring elsewhere for a complete review [8–10].

The mass of the five elementary Higgs particles required from MSSM, the two CP-even (h, H), the one CP-odd A and the two charged one H^\pm , at tree level are fixed by two independent input parameters, the ratio of the two vacuum expectation values $\tan\beta$ and the pseudoscalar Higgs-boson mass m_A . A simple relation holds between these particle masses :

$$m_{H,h}^2 = \frac{1}{2}[m_A^2 + m_Z^2 \pm \sqrt{(m_A^2 + m_Z^2)^2 - 4m_A^2 m_Z^2 \cos^2 2\beta}] \quad (1)$$

$$m_{H^\pm}^2 = m_W^2 + m_A^2 \quad (2)$$

From eq.(1), using the recent precise m_W and m_Z [11] measurements, m_h , the mass of the lightest Higgs neutral boson can be derived as a function of two parameters. Then, in this simple, lowest order approximation, the parametrization of the model concerning Higgs sector is performed through two free parameters $\tan\beta$ and m_A . At lowest order the light scalar Higgs mass, m_h , is smaller than m_Z , but including the radiative corrections, can be pushed up to about 135 GeV [12–17].

In the most general MSSM are necessary more free parameters than in the SM. Moreover the assumption that the scalar fermions masses, the gauginos masses and the trilinear Higgs-fermion couplings must unify at Grand Unification scale, GUT, reduces the number of free parameters. In one of the possible constrained model the parameters chosen are:

- M_{SUSY} , sfermion mass at the Electroweak scale.
- M_2 , $SU(2)_L$ gaugino mass at the Electroweak scale.
- μ , supersymmetric Higgs boson mass parameter.
- $\tan\beta$, the ratio of the two Higgs fields doublets.
- A_0 , a universal trilinear Higgs-squarks coupling at the Electroweak scale. It is assumed to be the same for up-type squarks and for down type squarks.
- m_A , mass of CP-odd Higgs boson.
- $m_{\tilde{g}}$, gluino mass. It affects loop corrections from stop and sbottom.

For Higgs search, two extremes of scalar top mixing are considered: maximal mixing $A_0 = \sqrt{6}$ TeV, and minimal mixing, when A_0 is zero. Usually a set of benchmarks are set and also in this case there are only two free parameters: $\tan\beta$ and m_A . In this search three benchmark scenarios are considered (Tab.1).

It is possible summarize the characteristics of the tree scenarios:

- m_h^{max} scenario.

It is designed to yield, as the name indicates the, maximum value of m_h in the model. The value of m_h can reach 135 GeV. It is the most conservative range of excluded $\tan\beta$ values for fixed values of the top quark and M_{SUSY} . A negative search of the h boson in such scenario implies an exclusion of the model.

Parameter (GeV)	1. m_h^{\max}	2. no mixing	3. large μ
M_{SUSY}	1000	1000	400
μ	-200	-200	1000
M_2	200	200	400
$X_t = A_t - \mu \tan \beta$	$2M_{\text{SUSY}}$	0	-300
m_g	$0.8M_{\text{SUSY}}$	$0.8M_{\text{SUSY}}$	200
m_A	4-1000	4-1000	4-1000
$\tan \beta$	0.4-50	0.4-50	0.4-50

Table 1: Benchmark scenarios

- *no mixing* scenario.

It assumes that there is no-mixing between the scalar partners of the left-handed and the right-handed top quarks. The highest value of m_h can be 114 GeV.

- *Large μ* . The third scenario is designed to illustrate choice of MSSM for which the Higgs h boson doesn't decay into pairs of b quarks due to large corrections from SUSY loop processes [18]. The effective Yukawa Higgs-bottom coupling is modified by radiative corrections involving SUSY-loops. The most considerable contributions come from the diagrams containing a vertex loop (gluino-sbottom, and higgsino-stop). Under certain conditions (specific choice of the SUSY parameters) these two diagrams destructively interfere with the tree level diagram $h \rightarrow b\bar{b}$ leading to the suppression of the $h \rightarrow b\bar{b}$ branching ratio. The dominant decay mode for these models are to $c\bar{c}$, gg, W^+W^- , $\tau^+\tau^-$. The highest value of m_h can be 108 GeV.

This work is focused on the first scenario as the most promising for the search of h boson due to the relatively high value of predicted m_h .

3 Experimental Status

In the past decade the data collected at LEP gave the most important contribution to the Standard Model test and its supersymmetric extension. The huge amount of high quality data allowed the performing high precision tests on the Standard Model and to investigate the validity of the Minimal Supersymmetric Standard Model. In particular the MSSM has been studied in representative scans of the parameters and mass limits on the existence of

the Higgs bosons have been set. The combined limit on the charged H^\pm and the neutral H bosons masses [5, 6] obtained are:

$$m_H > 114.4 \text{ GeV} \quad m_{H^\pm} > 78.6 \text{ GeV} \quad (3)$$

In addition, the four LEP experiments ALEPH [19], DELPHI [20], L3 [21], OPAL [22] performed a search of neutral CP-even and CP-odd Higgs bosons. This search has been carried through the study of the two most important production mechanisms of the light neutral Higgs boson in e^+e^- collisions :

$$e^+e^- \rightarrow hZ, \quad (4)$$

$$e^+e^- \rightarrow hA, \quad (5)$$

with the tree level cross sections related to the Standard Model Higgsstrahlung cross section, σ_{HZ}^{SM} , as [10]:

$$\sigma_{hZ} = \sin^2(\beta - \alpha)\sigma_{HZ}^{\text{SM}}, \quad (6)$$

$$\sigma_{hA} = \cos^2(\beta - \alpha)\tilde{\lambda}\sigma_{HZ}^{\text{SM}}, \quad (7)$$

where $\tan\beta$ is the ratio of the vacuum expectation values of the two Higgs doublets, α is the mixing angle in the CP-even Higgs boson sector and $\tilde{\lambda}$ is the p-wave suppression factor depending on the Higgs boson masses, m_h and m_A , and the centre-of-mass energy \sqrt{s} .

For most of the MSSM parameter space considered at LEP energies, the neutral Higgs bosons are predicted to decay dominantly into $b\bar{b}$ and $\tau^+\tau^-$. However, in certain parameter regions, other decays like $h \rightarrow AA$ and $A \rightarrow c\bar{c}$ become important. This search for the neutral Higgs bosons has been performed in the framework of the constrained MSSM (Sec. 2).

No indication of signal was found in the combined data at center-of-mass energies up to 209 GeV [7] and lower limits on the Higgs boson masses were set as function of $\tan\beta$ for several scenarios (Fig. 1). The mass limits obtained are:

$$m_h > 91.0 \text{ GeV} \quad m_A > 91.9 \text{ GeV} \quad (8)$$

In the m_h^{max} scenario, designed to extend the search to the maximal theoretical bound of m_h for any value of $\tan\beta$, the LEP data don't exclude the parameter space at $\tan\beta$ larger than 10, and with $m_A \sim 92 \text{ GeV}$ (Fig. 1).

A natural continuation of the LEP physics is the investigation of the possible existence of the CP-even h Higgs boson in this region of m_A and $\tan\beta$. The new Large Hadron Collider (LHC), under construction at CERN,

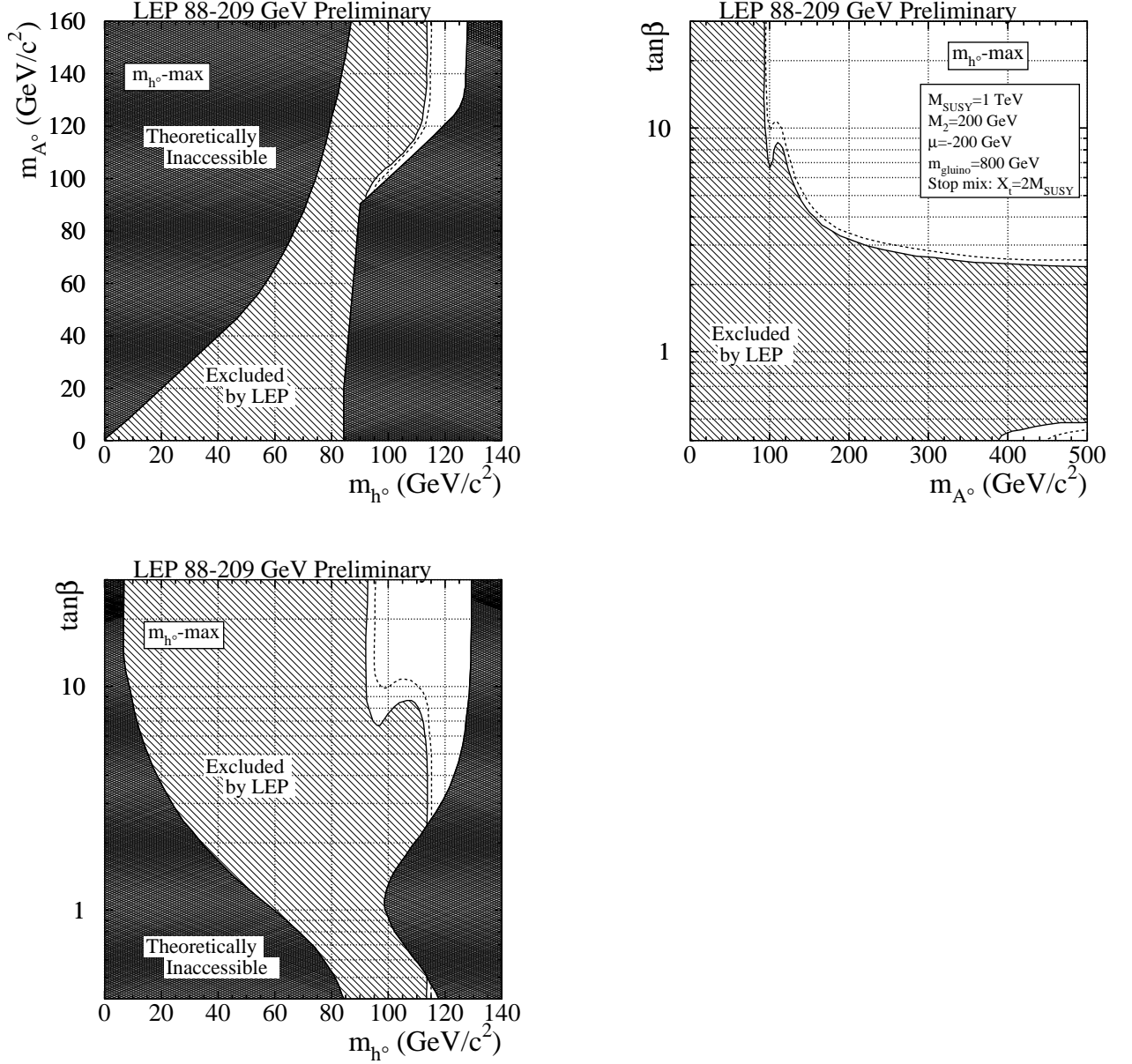


Figure 1: The combined LEP results for the search of the MSSM neutral Higgs bosons [7]. The MSSM exclusion plot for the m_h -max scenario. This figure shows the excluded (diagonally hatched) and theoretically disallowed (cross-hatched) regions as a function of the MSSM parameters in three projections: upper left in the (m_h, m_A) plane, upper right in the $(m_H, \tan\beta)$ plane, lower left in the $(m_A, \tan\beta)$ plane. The dashed lines indicate the boundaries of the regions expected to be excluded at 95% CL if only SM background processes are present. The difference between expected and observed limits are due to a slightly excess of events in experimental data compared to SM expectations [7].

and the experiments CMS [23] and ATLAS [24], will constitute a fantastic laboratory for such search.

The exploration of the parameter space, with the discovery of a Higgs supersymmetric Higgs boson or the rule out of this model, at least in this constrained scenario, constitutes the motivation of the analysis described in this paper.

The extraction of the h signal from the competing enormous background of Z decays, in the region of m_h close to m_Z constitutes a challenging search where all performances of the experimental setup have to be exploited and the most sophisticated analysis tools have to be used.

4 Minimal Supersymmetric Standard Model Higgs search at hadron collider

The prospect for the detection of the MSSM Higgs boson at LHC have been recently evaluated [24–26] for three set benchmark scenarios, for which supersymmetric (SUSY) particle masses are larger, preventing the Higgs Boson decays in SUSY particles. The interest was focused on discovery potential of various decay modes accessible also in case of the SM Higgs boson: $h \rightarrow \gamma\gamma$, $h \rightarrow b\bar{b}$, $H \rightarrow ZZ \rightarrow 4l$. Others modes strongly enhanced at high $\tan\beta$ as $H/A \rightarrow \tau^+\tau^-$ $H/A \rightarrow \mu^+\mu^-$ have been investigated [24]. The conclusion of these studies is that the complete region of parameter space $m_A = 50 - 500$ GeV and $\tan\beta = 1 - 50$, should be accessible for Higgs bosons discovery by ATLAS experiment, already with a collected integrated luminosity $\int \mathcal{L} dt = 100 \text{ fb}^{-1}$. Over a large fraction of this parameter space, more than one Higgs boson and more than one decay mode would be detectable. The possibility of search in more than one final state will be an excellent proof in case of the signal discovery. An exhaustive summary of all these decay modes can be found in Ref. [24]. The most difficult region was identified as the moderate $\tan\beta$ where only the lightest Higgs boson would be observable.

The investigated decay channels of the h boson are the same as of the SM Higgs boson: $h \rightarrow \gamma\gamma$ and $h \rightarrow b\bar{b}$. As in the SM case the search for Higgs boson decay in $\gamma\gamma$ can also be performed using associated WH and $t\bar{t}H$ production. The expected MSSM rates for $h \rightarrow \gamma\gamma$ are generally suppressed with respect the SM case. However, they could also be slightly enhanced in a limited region of parameters space. In Fig. 2, the 5σ contour curve of this channel is shown. This channel requires an excellent mass $M_{\gamma\gamma}$ resolution and jet/ γ separation.

The search of the h boson in the decay mode $h \rightarrow b\bar{b}$ is performed anal-

ogously than in SM case. Only the $t\bar{t}h$ production followed by the $h \rightarrow b\bar{b}$ decay can be observed clearly above the background, provided the complete event is reconstructed. This channel, as in the SM case, requires an excellent b-tagging performance, since the extraction of the signal requires the identification of four b-jets.

In the MSSM case, the rates can be enhanced by 10-20 % compared to the SM case. The signal observability in this case is reported as a 5σ discovery curve in Fig. 2.

From Fig. 2 it is clear that the region of m_h approximately 100 GeV and $\tan\beta$ greater than 10 has not been studied in other decay channels of the h boson. This circumstance has encouraged the work described in the following sections.

In the most general case considering all MSSM Higgs bosons, this region in the $m_A, \tan\beta$ plane is only accessible to the neutral boson H decay in $\mu^+\mu^-; \tau^+\tau^-$ and to charged bosons decay $H^\pm \rightarrow \tau\nu$. Having the possibility to observe also the lightest Higgs boson will be an essential proof of the model validity.

The channel $b\bar{b}h \rightarrow \mu^+\mu^-$ is a good channel to explore this region and requires at the same time an excellent performance in μ detection and in b-tagging. The ATLAS experiment has been designed with high demanding requests for the muon spectrometer and the inner detector.

5 Data sample

5.1 The lightest Supersymmetric Higgs boson

The neutral h boson and the others Higgs bosons are the important elements of the MSSM model. Their couplings to fermions and massive gauge bosons are easily obtained from the SM Higgs couplings, shown in Tab. 2 [26]. These correction factors multiplied by factors containing α and β (Sect. 2) are summarized in Tab. 3 [26]. The parameter α is the mixing angle required to diagonalize the Higgs mass matrix and is given by the following expression:

$$\cos 2\alpha = -\cos 2\beta \frac{m_A^2 - m_Z^2}{m_H^2 - m_h^2}, \quad (9)$$

At high $\tan\beta$, the correction factors to the MSSM h boson couplings relative to the SM couplings to fermions and massive gauge bosons (see Tab. 3)

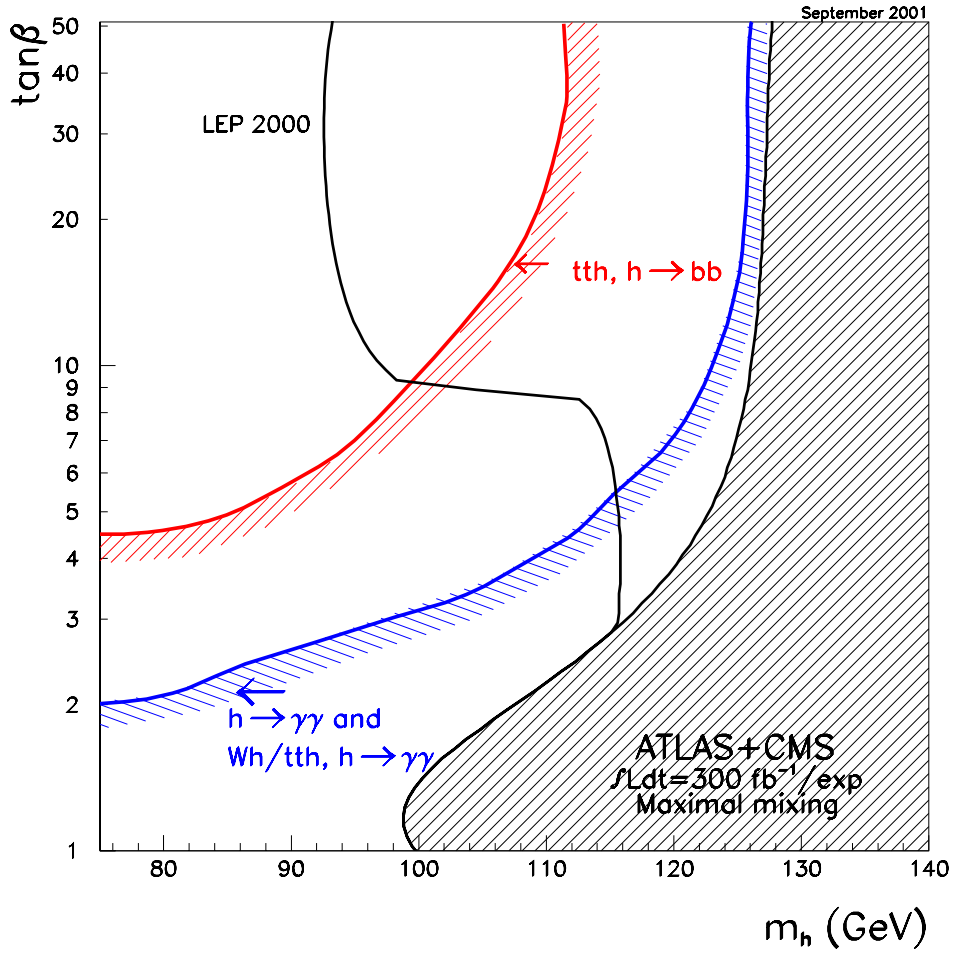


Figure 2: The ATLAS+CMS sensitivity for the discovery of the MSSM Higgs boson h , in case of maximal mixing. The 5σ discovery contour curves are shown in the $(\tan\beta, m_h)$ plane for the individual channels discussed and for an integrated luminosity of 300 fb^{-1} . The LEP limits are included. The forbidden region is shown diagonally hatched [27].

SM	Fermions	WW	ZZ
H	$\frac{igm_f}{2m_W}$	$igm_W g^{\mu\nu}$	$\frac{igm_Z}{2\cos\theta_W} g^{\mu\nu}$

Table 2: Standard Model Higgs couplings to fermions and massive gauge bosons.

MSSM	$d\bar{d}, s\bar{s}, b\bar{b}$ $e^+e^-, \mu^+\mu^-, \tau^+\tau^-$	$u\bar{u}, c\bar{c}, t\bar{t}$	WW, ZZ
h	$-\sin\alpha/\cos\beta$	$\cos\alpha/\sin\beta$	$\sin(\beta-\alpha)$
H	$\cos\alpha/\cos\beta$	$\sin\alpha/\sin\beta$	$\cos(\beta-\alpha)$
A	$-i\gamma_5 \tan\beta$	$-i\gamma_5 \cot\beta$	0

Table 3: MSSM correction factors to Higgs boson couplings with respect to SM couplings to fermions and massive gauge bosons.

are larger for down-type quarks (b) and leptons (τ and μ) than for up type-quarks. This fact implies that the coupling to down-type quarks are strongly enhanced in this region. Having the same couplings of the SM Higgs, the most natural choice is to explore the same decay channels: $h \rightarrow \gamma\gamma$ and $h \rightarrow b\bar{b}$, extensively studied (Sect. 4), Fig. 2, [24]. Others decays channels deserving consideration are the $h \rightarrow \tau^+\tau^-$ and $h \rightarrow \mu^+\mu^-$. The ratio couplings of the SM Higgs to the τ , μ fermions (see Tab. 2) are proportional to $(\frac{m_\tau}{m_\mu})^2$, consequently the heavy mass final state are favored. This apparent advantage is counterbalanced by the difficulty to identify the hadronic decay of τ -jet in hadronic events, by a smaller acceptance of the detector and by a worse mass resolution due to the presence of neutrinos in the final state.

Instead, a final state containing μ , as $h \rightarrow \mu^+\mu^-$, exploits the excellent combined performance of the muon spectrometer [28] and inner detector [29], compensating the smaller branching ratio with respect of the decay mode

$h \rightarrow \tau^+ \tau^-$.

To reduce the competing background it is better to perform the search for the $h \rightarrow \mu^+ \mu^-$ decay mode in a channel with two b-jets in the final state. The associated $b\bar{b}h$ production proceeds by the Yukawa bh coupling, which is enhanced at high $\tan\beta$, corresponding to higher cross section. Then the $b\bar{b}h$ production constitutes the dominant production of h boson in high $\tan\beta$ region. In Fig. 3 and Fig. 4 the Feynman diagrams contributing to the process $gg \rightarrow h b \bar{b} \rightarrow \mu^+ \mu^- b \bar{b}$ and $q\bar{q} \rightarrow h b \bar{b} \rightarrow \mu^+ \mu^- b \bar{b}$ are represented.

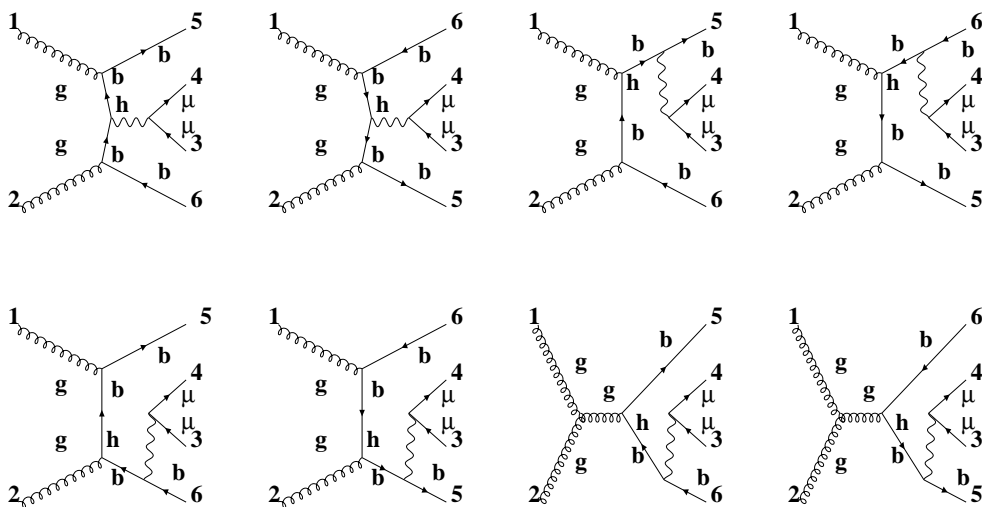


Figure 3: Diagrams contributing, at “tree level”, to the process $gg \rightarrow h b \bar{b} \rightarrow \mu^+ \mu^- b \bar{b}$.

Before concluding this section it should be reminded [26] that the CP-odd supersymmetric boson A in this region of high $\tan\beta$ and m_h approximately 100 GeV has a mass slightly higher than the CP-even, h, and competitive branching ratio (Tab. 3) in the corresponding decay channel $A \rightarrow \mu^+ \mu^-$. The cross-section, the mass and width difference, which are functions of the parameters $\tan\beta$ and m_A are close in some points of the parameters space (Sect. 6.1). Then in these points the CP-odd and CP-even bosons are indistinguishable from the experimental point of view. Then it is more correct to discuss about h/A search. It is possible to summarize the purpose of this paper search for h/A boson as a sign to the discovery of Supersymmetry. Nevertheless, it has to be paid attention that the couplings to heavy bosons and fermions of these two bosons are different.

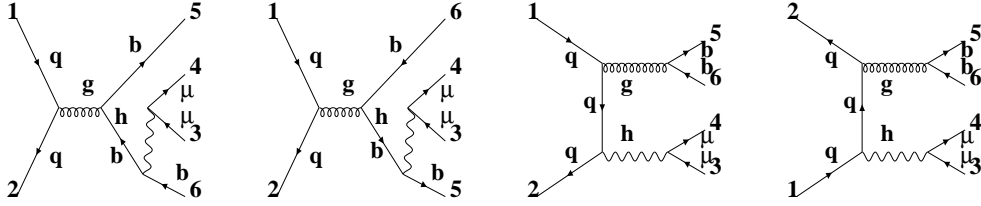


Figure 4: Diagrams contributing, at “tree level”, to the process $q\bar{q} \rightarrow h b \bar{b} \rightarrow \mu^+ \mu^- b \bar{b}$.

In the following paragraphs the A boson contribution to the signal is taken in account, but shortly is indicated as h/A boson.

5.2 Background processes

Others processes have the same final state, a μ -pair and two b-jets, as the signal. These reactions, constituting the background of the h search, have higher production cross-sections than the signal. Then, it has to be payed a lot of effort in controlling and understanding them.

The main background is originated from the Z/γ^* production with two b-jets and a subsequent decay into a μ -pair. The cross section of this process is a few order of magnitude greater than the signal. Namely, the cross section times the branching ratio, $\sigma \cdot \text{Br}(Z \rightarrow \mu^+ \mu^-)$, is approximately 1500 pb, with two quarks in the event, as evaluated from PYTHIA 6.203 (with $m_Z > 80$ GeV). This cross section has to be compared with a typical value of the signal, $\sigma \cdot \text{Br}(h \rightarrow \mu^+ \mu^-) \approx 0.1$ pb, at $\tan\beta = 30$ and $m_h = 110$ GeV).

In Fig. 5 and Fig. 6 diagrams corresponding to Z productions are illustrated.

Comparing the Fig. 3, Fig. 4 and Fig. 5, Fig. 6, it is clear the two sets of diagrams are similar provided to replace the h of the signal with a Z boson. The distinction between the signal from the background when m_h is approaching to m_Z is an extremely hard task due to the similar topologies of the decays.

Another background that contributes to the same final state is the ZZ associated production, followed by one Z decaying into $b\bar{b}$ and the second one decaying into $\mu^+ \mu^-$. The cross section of this process is negligible, $\sigma \cdot \text{Br}(Z \rightarrow \mu^+ \mu^-) \cdot \text{Br}(Z \rightarrow b\bar{b}) \approx 0.15$ pb [30], compared to the main background. Nevertheless is of the same order of magnitude as the signal. The contribution

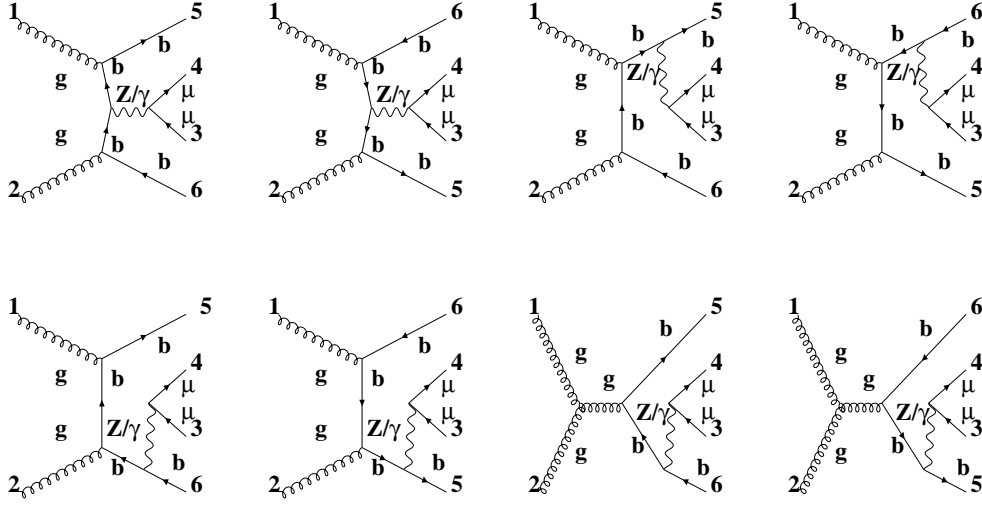


Figure 5: Subset of the diagrams contributing, at “tree level”, to the process $gg \rightarrow Z/\gamma^* b\bar{b} \rightarrow \mu^+ \mu^- b\bar{b}$.

of this background is, as will be discussed in the following paragraphs, easily suppressed using kinematic characteristics of these events.

Another process contributing to the same final state is the associated production of two t quarks $t\bar{t}$ (Fig. 7), followed by a top-quark decay in a b -quark and a W boson and a subsequent W decay in $\mu\nu$. This cross section times the branching ratios is approximately $\sigma(t\bar{t}) \cdot \text{Br}(t \rightarrow bW) \cdot \text{Br}(W \rightarrow \mu\nu) \cdot \text{Br}(t \rightarrow bW) \cdot \text{Br}(W \rightarrow \mu\nu) \approx 5.84\text{pb}$ [30].

The presence of two neutrinos implies a missing energy in the event, as will be discussed in the following paragraphs, and this characteristic is used to strongly reduce this background. Naively, it can be thought to discriminate the signal from this background on the basis of the different b -jets characteristics. In fact, the two b -jets of this background events are usually more energetic than those accompanying the signal; consequently the probability of their identification is higher. This implies a simple consideration: requiring the identification two b -jets won’t enhance the signal over this specific background, because this requirement will suppress more the signal than this background.

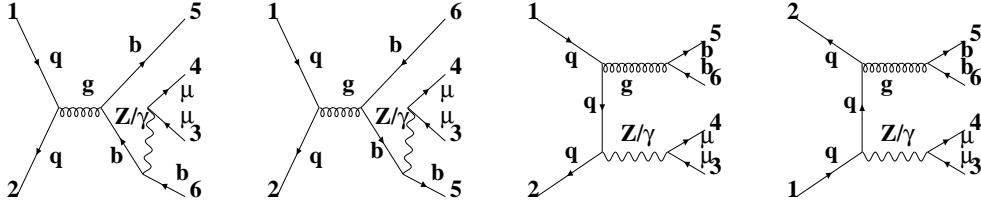


Figure 6: Diagrams contributing, at “tree level”, to the process $q\bar{q} \rightarrow Zb\bar{b} \rightarrow \mu^+\mu^-b\bar{b}$.

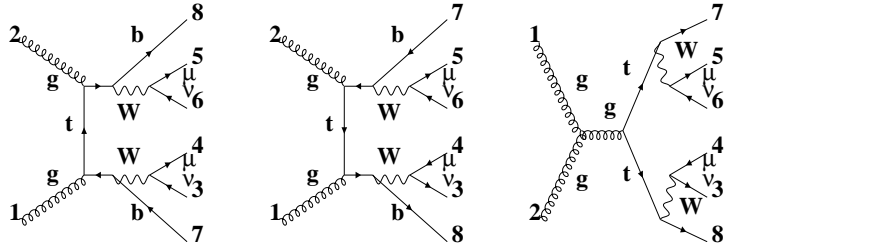


Figure 7: Diagrams contributing, at “tree level”, to the process $t\bar{t} \rightarrow \mu^+\mu^-b\bar{b}$; the diagram including quarks fusion is obtained from third diagram replacing the two gluons with incoming. Its contribution to the cross section is $\approx 10\%$.

6 Monte Carlo Simulation: Fast and Full Simulation in ATLAS detector

To exploit all discovery potential of ATLAS detector for the neutral h boson in the process $pp \rightarrow b\bar{b}h \rightarrow b\bar{b}\mu^+\mu^-$ and design the best strategy to extract this signal from background, as discussed in Sec. 6.1, a huge number of events have to be generated and simulated in the detector. This task can be performed using a “full simulation” of the detector, that is taking into account detailed descriptions of the geometry of all active and passive elements and of their interactions with particles originating from the pp collisions. An alternative method, which is less detailed but more efficient in terms of computing time consuming, consists in “fast simulation” and is based upon parameterizations of the detector performances.

To choose the appropriate simulation [31] in the h search performances of the two methods are compared in the study of the channel $h \rightarrow \mu^+\mu^-$ in the pseudorapidity acceptance of Inner Detector and Muon Spectrometer $|\eta| < 2.5$. In this comparison attention is mainly pointed to the two detectors more relevant for this channel, the Inner Detector and the Muon Spectrometer, and specifically in studying the performance of combined reconstruction.

The event generation has been performed using PYTHIA6.203 [30] Monte Carlo with MSSM parameters $m_h=100$ GeV and $\tan\beta=20$. Then data simulation has been performed using both methods: the ATLAS “fast simulation” package ATLFAST 2.60 [32], and the GEANT3-DICE “full simulation” package together with MuonBox and XKalman reconstruction packages and STACO algorithm for the combination of the reconstructions in the two sub-detectors.

Results from simulation in combined reconstruction mode are shown in Fig. 8 and in Fig. 9 respectively for “full simulation” and “fast simulation” methods. In the upper part of Fig. 8, the invariant mass of the μ -pairs is shown as generated from Monte Carlo and as reconstructed from the Inner Detector and Muon Spectrometer, in the lower part, their difference, $M_{\text{rec}} - M_{\text{gen}}$, is plotted with superimposed the fit results with a gaussian function. The significant parameters values are the mean value, $\mu = -0.17 \pm 0.02$ and the sigma, $\sigma = 1.58 \pm 0.02$ GeV.

In the upper part of Fig. 9, the invariant mass of the μ -pairs is plotted and the difference of reconstructed and generated mass with the fitted function superimposed in the lower section, with parameters values: the mean value, $\mu = 0.039 \pm 0.018$ GeV and the sigma, $\sigma = 1.33 \pm 0.01$ GeV.

An estimate of the reconstruction efficiency convoluted with the detector acceptance has been performed in the two cases giving compatible values of 75%.

A comparison on the resolution in the reconstruction of the most significative variables as transverse momentum, $\sigma_{P_T}^{\mu\mu}$, pseudorapidity, $\sigma_{\eta}^{\mu\mu}$, azimuthal angle, $\sigma_{\phi}^{\mu\mu}$ and mass $\sigma_m^{\mu\mu}$ of the μ -pairs is summarized in Tab.4.

The results obtained are encouraging the use of “fast simulation”, ATLFAST, in the following $h \rightarrow \mu^+\mu^-$ analysis.

6.1 Events Simulation

The efficiency of the selection criteria, the detector acceptance and the purity of the data sample are estimated using Monte Carlo events for the signal $b\bar{b}h \rightarrow \mu^+\mu^-$ with two b-quarks and the main backgrounds ($t\bar{t}$, Zjet-jet, ZZ) generated by the PYTHIA program [30]. The events are then passed through the ATLAS detector fast simulation ATLFAST [32].

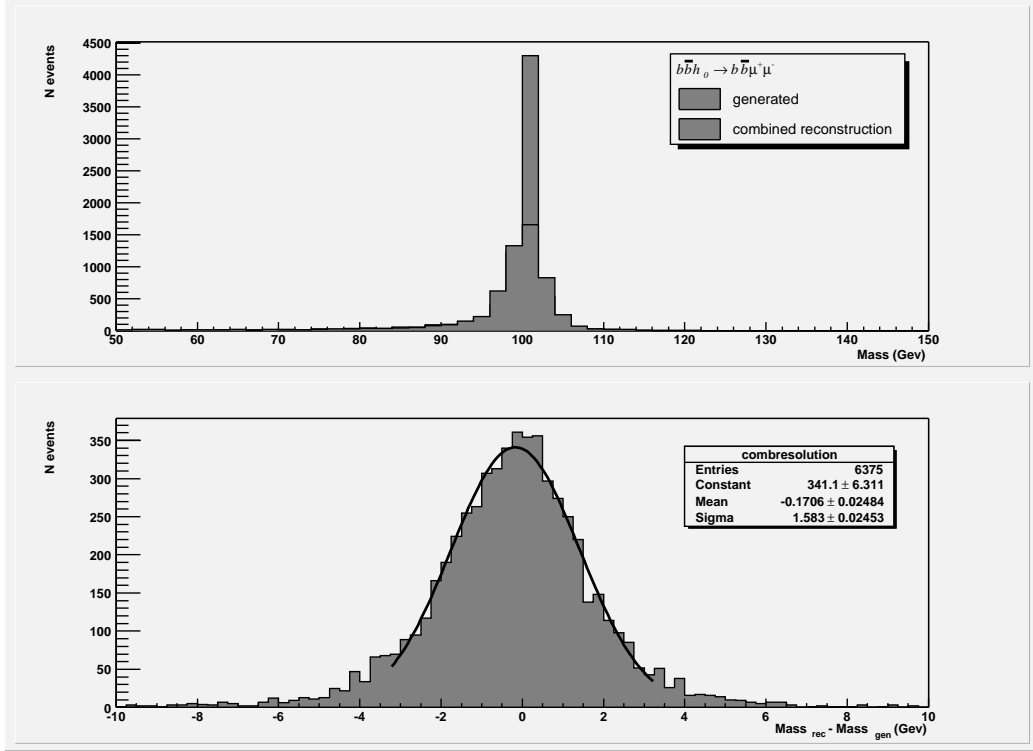


Figure 8: Mass resolution of the μ -pair from combined reconstruction of Inner Detector and Muon Spectrometer in the process $h \rightarrow \mu^+ \mu^-$ and two b-jets in maximal mixing scenario ($m_h = 100$ GeV, $\tan\beta=20$). The plots are obtained using the full simulation of ATLAS detector (see text). On the top part: μ -pairs invariant mass distribution, as generated by Monte Carlo (horizontal hatched) with over-lined the corresponding distribution as obtained combining the reconstructions in the two detectors (dots). On the bottom part: difference between the reconstructed and generated invariant mass, ($M_{\text{rec}} - M_{\text{gen}}$). The black line is representing fit with a gaussian function $f(x) = p_0 \cdot \exp(-0.5 \cdot (\frac{x-p_1}{p_2})^2)$ with parameters ($p_0 = 341 \pm 6$ GeV, $p_1 = -0.17 \pm 0.02$ GeV e $p_2 = 1.58 \pm 0.01$ GeV).

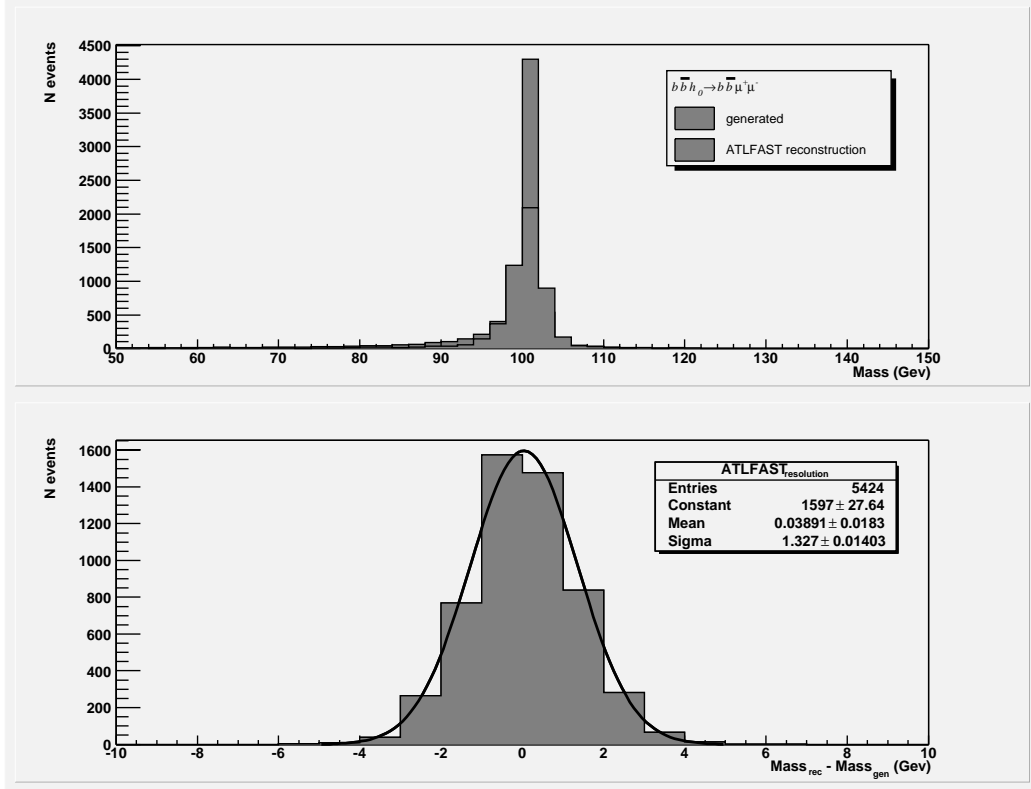


Figure 9: Mass resolution of the μ -pairs from combined reconstruction of Inner Detector and Muon Spectrometer in the process $h \rightarrow \mu^+ \mu^-$ and two b-jets in maximal mixing scenario ($m_h = 100$ GeV, $\tan\beta = 20$). The plots are obtained using the fast simulation of ATLAS detector, ATLFAST (see text). On the top part: μ -pairs invariant mass distribution as generated by Monte Carlo (horizontal hatched) with over-lined the corresponding distribution after reconstruction in the detector (dots). On the bottom part: difference between the reconstructed and generated μ -pairs invariant mass, ($M_{\text{rec}} - M_{\text{gen}}$). The black line is representing fit with a gaussian function $f(x) = p_0 \cdot \exp(-0.5 \cdot (\frac{x-p_1}{p_2})^2)$ with parameters ($p_0 = 1597 \pm 28$ GeV, $p_1 = 0.039 \pm 0.018$ GeV e $p_2 = 1.33 \pm 0.01$ GeV).

	$\sigma_{p_T}^{\mu\mu}$	$\sigma_{\eta}^{\mu\mu}$	$\sigma_{\phi}^{\mu\mu}$	$\sigma_m^{\mu\mu}$	$\epsilon_{2\sigma}$
Full simulation	13%	10%	15%	1.58 ± 0.03 GeV	66%
Fast simulation	10%	7%	12%	1.33 ± 0.01 GeV	77%

Table 4: Resolution in transverse momentum, $\sigma_{p_T}^{\mu\mu}$, pseudorapidity, $\sigma_{\eta}^{\mu\mu}$, azimuthal angle, $\sigma_{\phi}^{\mu\mu}$, and mass $\sigma_m^{\mu\mu}$, of the μ -pair, $\epsilon_{2\sigma}$, efficiency inside 2σ window, in case of “full simulation” of ATLAS detector and “fast simulation”, using ATLFAST.

The analysis has been performed in high luminosity scenario when LHC will reach a luminosity of $\mathcal{L} = 10^{-34} \text{ cm}^{-2}\text{s}^{-1}$, after data collection corresponding to an integrated luminosity of $\int \mathcal{L} dt = 300 \text{ fb}^{-1}$.

The signal, $bb h \rightarrow \mu^+ \mu^-$, has been simulated in 56 points of parameter space ($\tan\beta$, m_h), corresponding to eight points in $\tan\beta$, chosen equally spaced between 15 and 50, in 5 step, and seven points in the m_h range between 95 GeV and 125 GeV, in 5 GeV step.

Due to the indistinguishable contribution of the CP-odd neutral Higgs, A, the decay $bbA \rightarrow \mu^+ \mu^-$ has been also simulated in 6 points of parameter space corresponding to the same eight points in $\tan\beta$ (15,50) and in seven points in the m_A range between 95 GeV and 125 GeV, in 5 GeV step.

The background events are considered originate from the following channels:

- $Z \rightarrow \mu^+ \mu^- + \text{jet-jet}$. The events have been generated in the m_Z region > 80 GeV. The event generation is limited to the region of interest of our channel, excluding the high cross section tail of events, not interesting for our studies. These events are in any case selected easily with the standard selection criteria.
- $ZZ \rightarrow b\bar{b}\mu^+\mu^-$. This background has been considered, but due to its low cross section, its importance is relatively low.
- $t\bar{t} \rightarrow W^+W^-b\bar{b} \rightarrow b\bar{b}\mu\nu\mu\nu$.

For all these channels a number of events corresponding to 5 times the expected number of data produced during the data taking has been generated.

In the fast simulation program ATLFASTB [32] is included a b-jet identification, b-tagging, with efficiency $\epsilon = 50$ %. The detector acceptance considered is $|\eta| = 2.5$. No trigger simulation is implemented; however the value

of transverse muon momentum, p_T^μ above experimental trigger threshold is required.

In Fig. 10 are represented the production cross section and the product of the production cross section times branching ratio for the neutral MSSM bosons decaying into a μ pair as function of m_h . In Fig. 11 are represented the variations as a function of m_h of the mass, width difference and ratio of h and A boson, and the width of the h boson.

The cross sections and the cross sections times the branching ratio, $\sigma \cdot \text{Br}(h \rightarrow \mu^+ \mu^-)$, for all these points are summarized in Tab. 5 and Tab. 6 respectively.

$\tan \beta$	15	20	25	30	35	40	45	50
m_h (GeV)								
95	0.132	0.238	0.371	0.541	0.725	0.949	1.209	1.470
100	0.113	0.203	0.320	0.451	0.632	0.827	1.034	1.273
105	0.094	0.172	0.277	0.396	0.545	0.705	0.899	1.113
110	0.079	0.148	0.236	0.344	0.468	0.614	0.772	0.959
115	0.062	0.122	0.196	0.290	0.403	0.524	0.671	0.833
120	0.038	0.084	0.148	0.227	0.323	0.437	0.567	0.709
125	0.004	0.014	0.033	0.068	0.129	0.202	0.302	0.424

Table 5: σ in nb, calculated by Pythia 6.203.

$\tan \beta$	15	20	25	30	35	40	45	50
m_h (GeV)								
95	0.035	0.063	0.099	0.142	0.193	0.251	0.317	0.361
100	0.030	0.054	0.085	0.122	0.167	0.217	0.274	0.337
105	0.025	0.046	0.073	0.106	0.145	0.189	0.239	0.294
110	0.021	0.040	0.063	0.092	0.126	0.164	0.208	0.257
115	0.017	0.033	0.053	0.078	0.108	0.142	0.181	0.223
120	0.010	0.023	0.040	0.062	0.087	0.118	0.153	0.190
125	0.001	0.004	0.009	0.019	0.035	0.055	0.081	0.115

Table 6: $\sigma \cdot \text{Br}(h \rightarrow \mu^+ \mu^-)$ in pb, calculated by Pythia 6.203.

The h width is summarized in Tab. 7 vs m_h , A width and m_A are reported in Tab. 8 vs m_h Tab. 9.

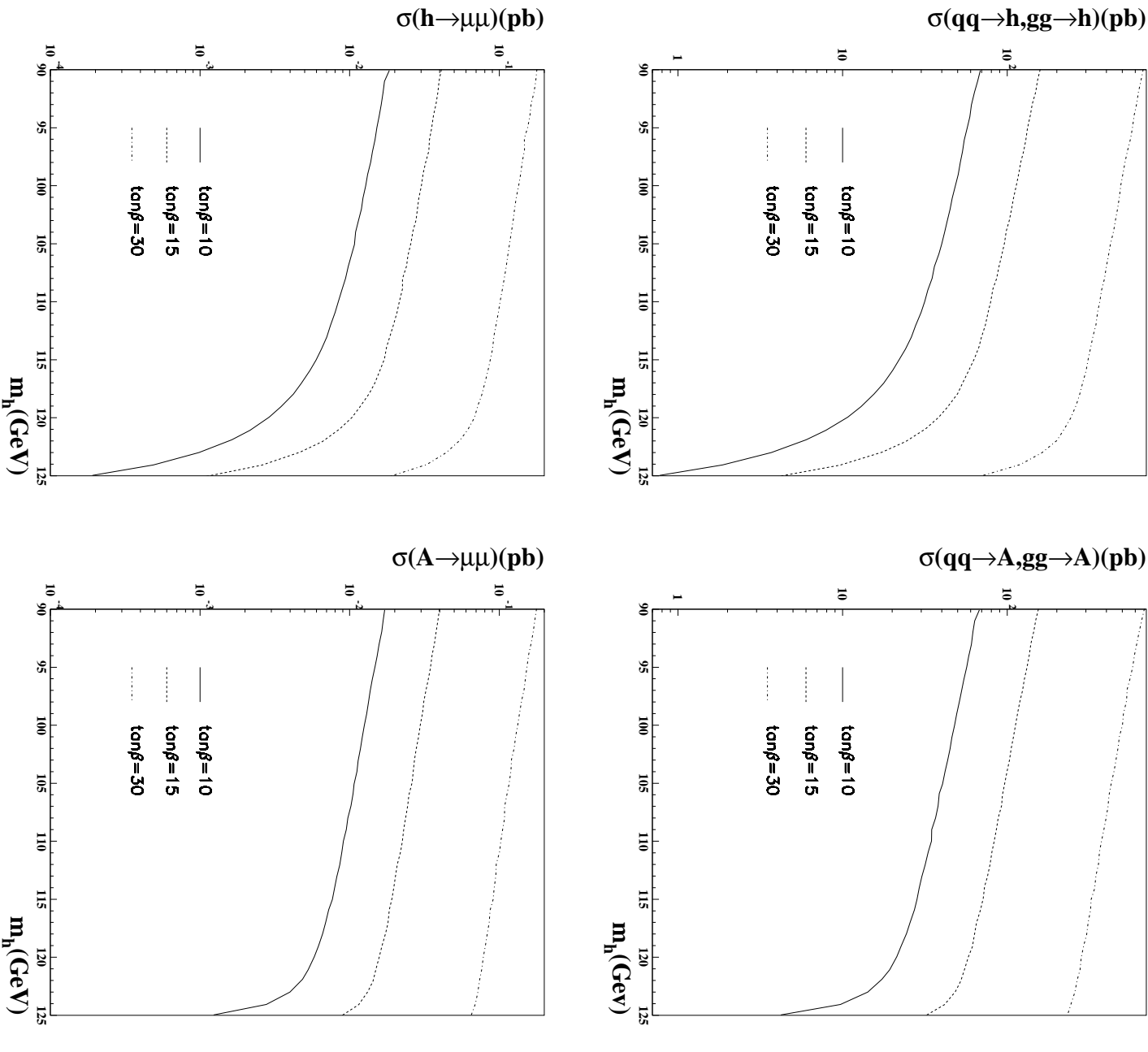


Figure 10: a) Production cross section of the neutral h boson in qq and gluon-gluon fusion (top left) b) Production cross section of the neutral A boson in qq and gluon-gluon fusion (top right) c) Production cross section of the neutral h boson times branching ratio in $\mu^+\mu^-$ (bottom left) d) Production cross section of the neutral A boson times branching ratio in $\mu^+\mu^-$ (bottom right). The solid, dashed and dashed-dotted line correspond to $\tan\beta$ values = 10, 15 and 30 respectively [30].

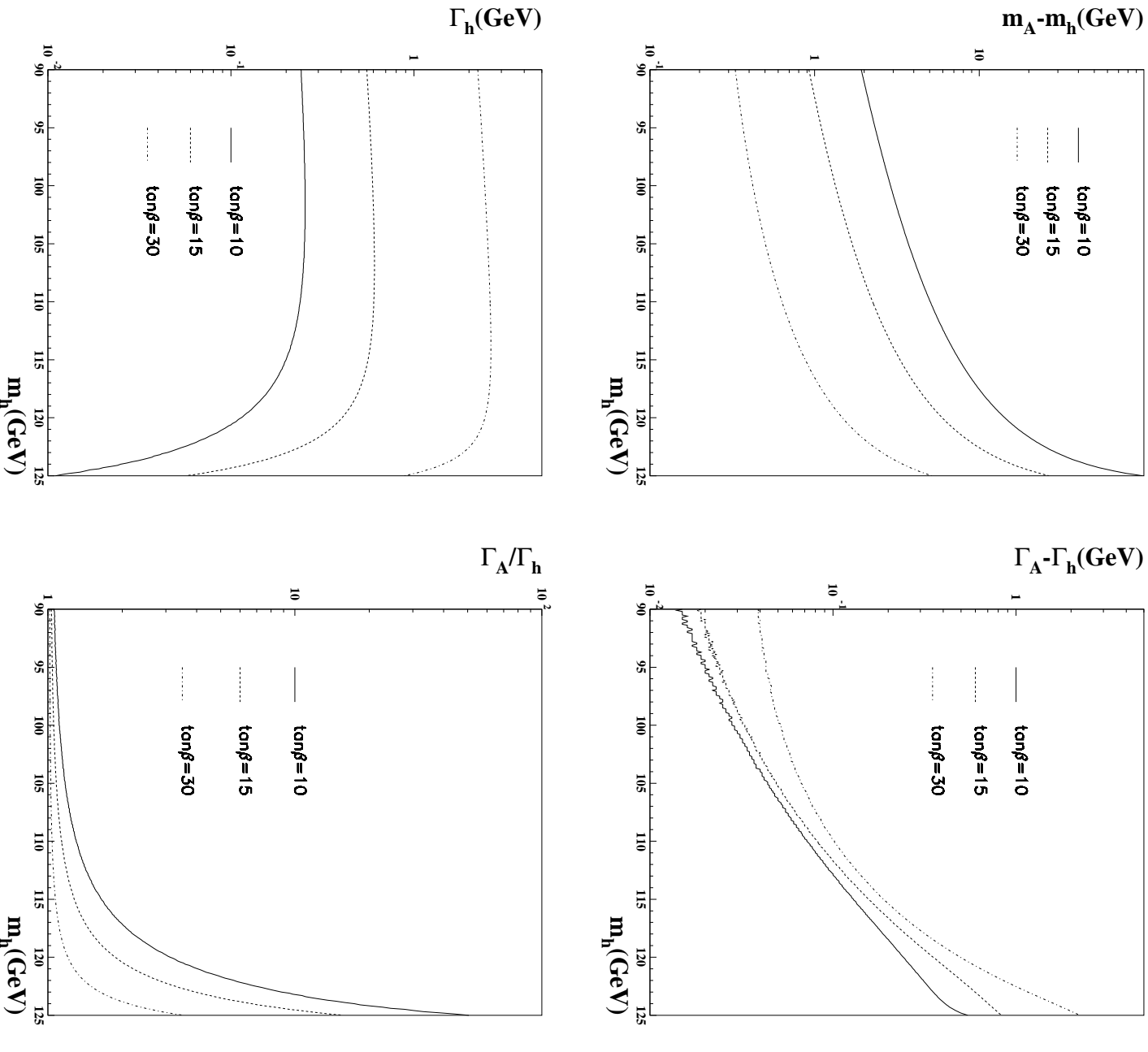


Figure 11: a) Mass difference between the neutral bosons A and h as a function of m_h (top left) b) Width difference between neutral bosons A and h as a function of m_h (top right) c) h boson width as a function of m_h (bottom left) d) Width ratio of the neutral bosons A and h as a function of m_h (bottom right). The solid, dashed and dashed-dotted line correspond to $\tan\beta$ value = 10, 15 and 30 respectively [30].

$\tan \beta$	15	20	25	30	35	40	45	50
m_h (GeV)								
95	0.574	1.028	1.613	2.328	3.175	4.152	5.259	6.496
100	0.592	1.069	1.682	2.430	3.314	4.337	5.495	6.789
105	0.605	1.101	1.740	2.525	3.447	4.512	5.722	7.074
110	0.602	1.117	1.783	2.597	3.559	4.672	5.930	7.339
115	0.560	1.088	1.776	2.621	3.623	4.780	6.090	7.557
120	0.405	0.899	1.581	2.430	3.455	4.659	6.035	7.557
125	0.052	0.186	0.413	0.857	1.598	2.533	3.744	5.318

Table 7: Neutral boson h width, calculated by Pythia 6.203.

$\tan \beta$	15	20	25	30	35	40	45	50
m_A (GeV)								
95	0.598	1.057	1.648	2.371	3.227	4.215	5.335	6.586
100	0.625	1.107	1.726	2.481	3.374	4.407	5.577	6.885
105	0.653	1.155	1.800	2.592	3.522	4.597	5.818	7.182
110	0.683	1.205	1.878	2.698	3.667	4.789	6.057	7.477
115	0.715	1.257	1.956	2.810	3.816	4.985	6.299	7.777
120	0.755	1.317	2.041	2.928	3.977	5.183	6.545	8.081
125	0.895	1.453	2.203	3.112	4.184	5.432	6.846	8.423

Table 8: Neutral boson A width, calculated by Pythia 6.203.

6.2 Event Selection

The study of the channel is performed considering the event topology $\mu^+\mu^-$. To cover the MSSM parameters regions where the decay $A \rightarrow \mu^+\mu^-$ becomes important, this channel is studied as well.

The signature of the $A/h \rightarrow \mu^+\mu^-$ with two b-quarks in the final state is two high energy muons and the presence of b hadrons. The invariant mass of the muons supposed to originate from h boson must be compatible, within mass resolution, with its mass, m_h . The signature is, also, characterized by two high multiplicity hadronic jets originating from b-quarks.

The main background, as discussed in the previous paragraph (Sec. 5.2), are the Z decays in $\mu^+\mu^-$. The selection criteria are optimized accordingly.

First, a preselection is applied which significantly reduces the background, while keeping a high signal efficiency; this is especially effective against background with low P_T muons. Then a further set of selection criteria is chosen to increase the signal-to-background ratio.

$\tan \beta$	15	20	25	30	35	40	45	50
m_h (GeV)								
95	96.2	95.6	95.4	95.3	95.3	95.3	95.3	95.3
100	101.3	100.9	100.6	100.4	100.3	100.3	100.3	100.3
105	106.6	105.9	105.6	105.6	105.4	105.3	105.3	105.3
110	112.3	111.2	110.9	110.6	110.4	110.4	110.3	110.3
115	118.2	116.8	116.2	115.9	115.6	115.6	115.4	115.4
120	125.9	123.2	122.	121.5	121.2	120.9	120.6	120.6
125	153.1	137.9	133.2	130.3	128.5	127.6	127.0	126.5

Table 9: Neutral boson A mass,calculated by Pythia 6.203.

A preselection is applied requiring events to have at least two well identified charged muons with $P_T > 10$ GeV and a pseudo-rapidity $|\eta| < 2.5$. The presence of a pair of b-jets with $P_T > 15$ GeV and $|\eta| < 2.5$ are required.

To further reject background events the transverse momentum, $P_T^{\mu 1}$, of the most energetic muon is required to exceed 25 GeV and not higher than 100 GeV. For the less energetic muon is instead required an upper bound for the $P_T^{\mu 2}$ at 60 GeV and the same lower limit. The $\mu^+ \mu^-$ invariant mass has to lie inside a window around h/A mass of 2.5 GeV. The transverse momentum of the b-jets has to be greater than 60 GeV for the most energetic and less than 55 GeV for the less energetic one. The missing transverse momentum of the event is required to be less than 25 GeV. These selection cuts are summarized in Tab. 10.

variable	lower limit GeV	upper limit GeV
$P_T^{\mu 1}$	25	100
$P_T^{\mu 2}$	25	60
$M_{\mu^+ \mu^-}$	$m_h - 2.5$	$m_h + 2.5$
$P_T^{b 1}$	60	
$P_T^{b 2}$	55	
P_T^{miss}	25	

Table 10: Selection criteria for A /h $\rightarrow \mu^+ \mu^-$ with two b-quarks final state.

Three samples with different b-tag characteristics are studied:

- **double b-tag.** Both b-jets are identified in the detector. All b-jets of event are considered.

- **at least one b-tag.** At least a b-jet is identified in the detector.
- **only one b-tag.** Only one b-jet is identified in the detector between the two most energetic jets.

From their definition is clear that these samples are not exclusives, *i.e.* the same event can belong to two different categories, *e.g.* events in the only one b-tag category can be also in the double b-tag sample.

The Tab. 11 reports the number of expected signal events for Higgs Boson mass $m_h=100$ GeV and $\tan\beta=40$ the number of background events for the background of $t\bar{t}+ZZ$ and $Z+jets$. The numbers shown in Tab. 11 are for the double b-tag samples. Tab. 12 and Tab. 13 are referring to sample of single b-tag and only b-tag.

For these choices of m_h and $\tan\beta$ the distribution of the two μ invariant mass, the transverse momentum distributions, the transverse momentum of most energetic μ and most energetic b-quarks are shown for the three different b-tag sample are shown in Fig. 12 double b-tag, in Fig. 13 at least one b-tag, in Fig. 14 only one b-tag.

Double b-tag sample. $m_h = 100$ GeV, $\tan\beta = 40$				
	$N_{h\rightarrow\mu\mu}$ $\cdot 10^{-3}$	$N_{t\bar{t}}$ $\cdot 10^{-4}$	N_{ZZ} $\cdot 10^{-3}$	N_{z+jets} $\cdot 10^{-4}$
N_{gen}	328	854	174	$241 \cdot 10^3$
presel.	10.5	363	33	256
$P_T^{\mu 1}$	8.3	258	25	212
$P_T^{\mu 2}$	6.3	141	18	157
$M_{\mu^+\mu^-}$	3.1	6.9	0.5	4.8
P_T^{b1}	2.3	1.9	0.4	4.1
P_T^{b2}	2.1	1.2	0.3	3.8
P_T^{miss}	2.1	0.9	0.3	3.8

Table 11: Double b-tag sample. The number of MC generated signal events, $N_{h\rightarrow\mu\mu}$, and the expected number of background events in the channel $t\bar{t}$, $N_{t\bar{t}}$, ZZ , N_{ZZ} , and Z with two jets N_{z+jets} , in the various step of selection: generated from MC, N_{gen} , after preselection (see text), after selections on the transverse momentum of the first and the second more energetic μ , $P_T^{\mu 1}, P_T^{\mu 2}$, on the μ pair invariant mass, $M_{\mu^+\mu^-}$, on the transverse momentum of the b-jets, P_T^{b1} and P_T^{b2} , and finally on the missing transverse momentum of the event, P_T^{miss} . The number are given for $m_h = 100$ GeV and $\tan\beta=40$ in the “single b-tag” sample (see text). The number of generated events corresponds to 5 times the expected integrated luminosity of $\int \mathcal{L} dt = 300 \text{ fb}^{-1}$.

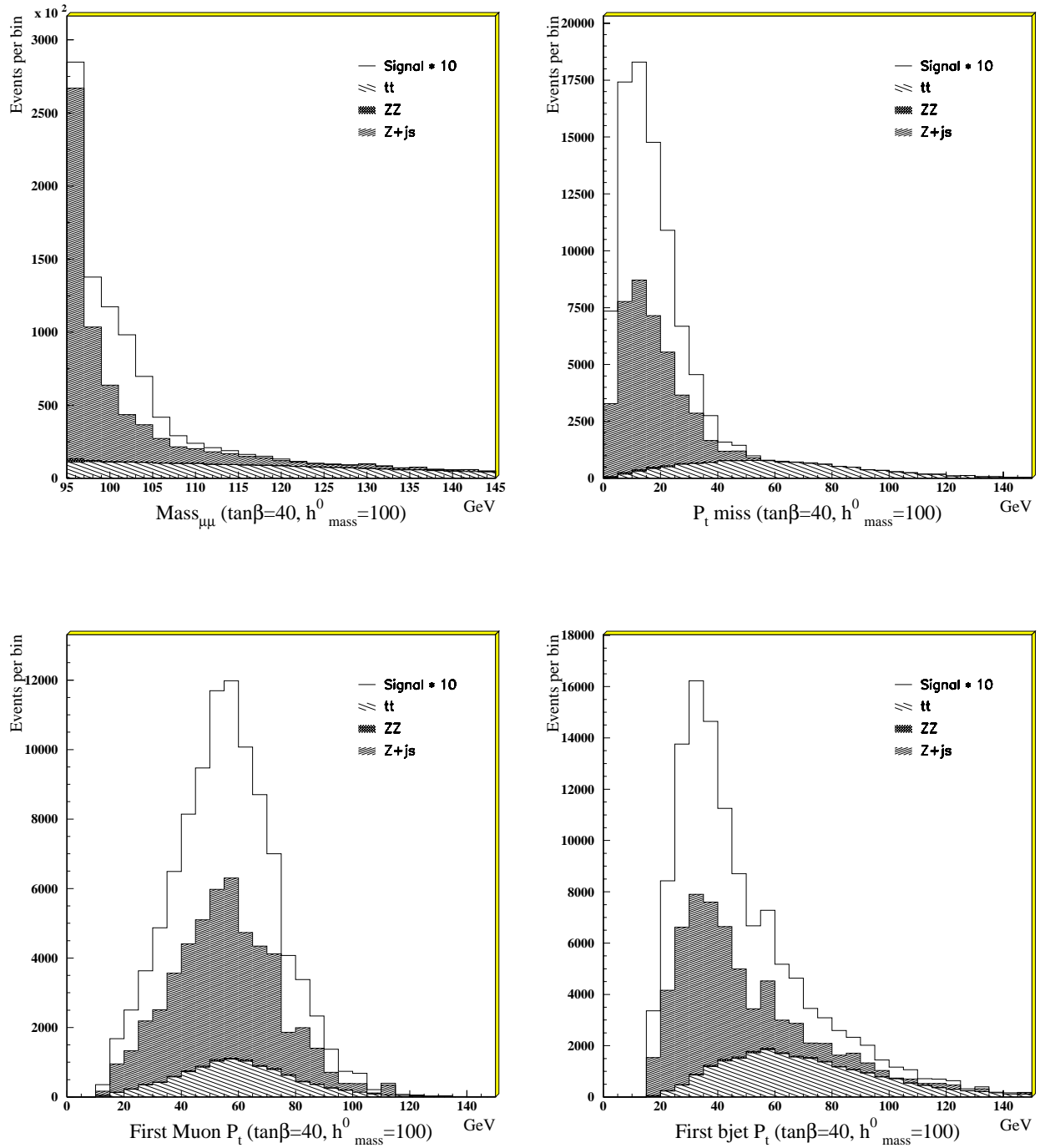


Figure 12: Distributions of the μ -pair invariant mass, of the total transverse missing momentum of the event, p_t missing, the most energetic μ transverse momentum and the most energetic b-quark transverse momentum, for the “double b-tag” sample. The distributions correspond to $\tan\beta = 40$ and $m_h = 100$ GeV [30].

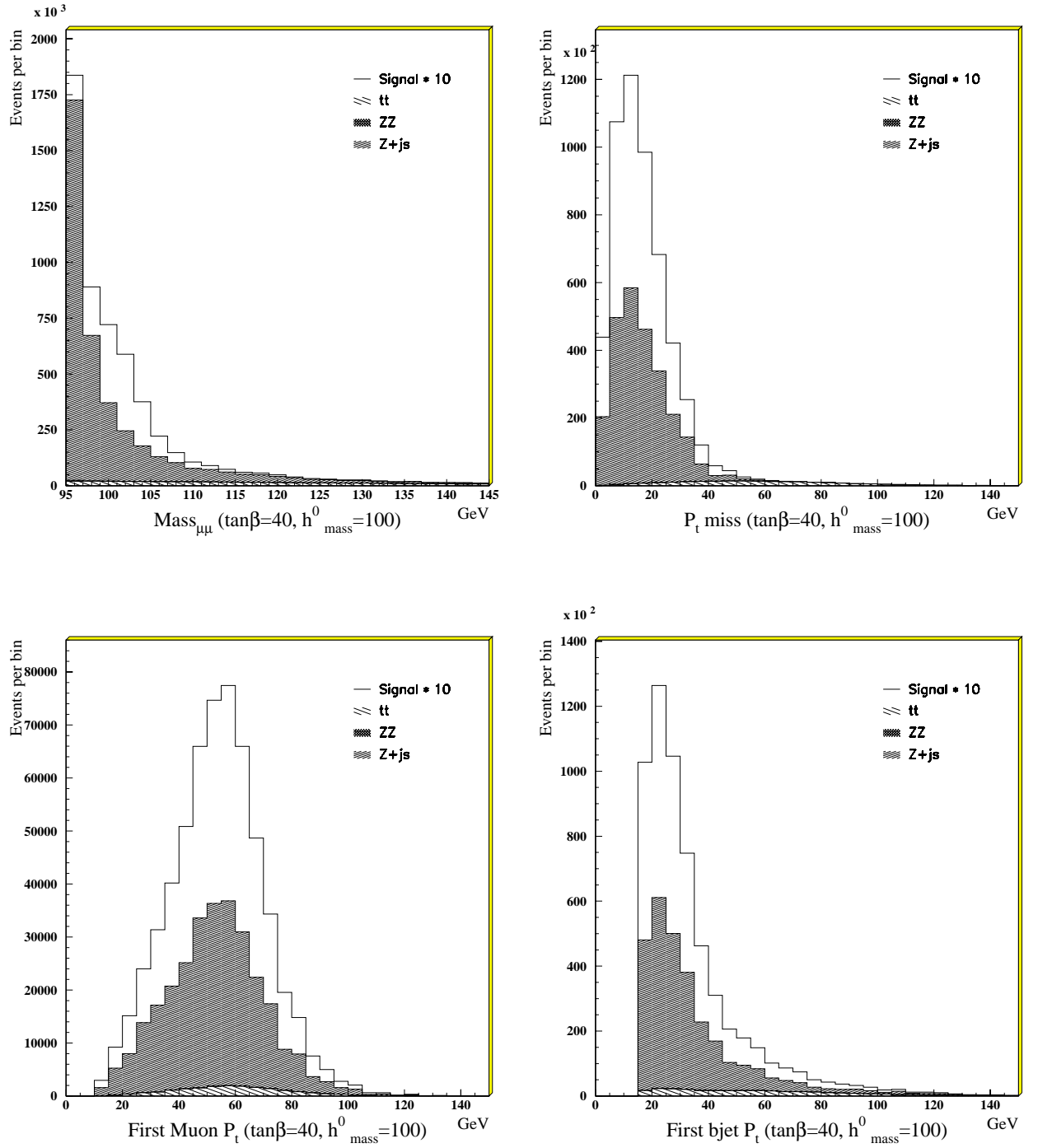


Figure 13: Distributions of the μ -pair invariant mass, of the total transverse missing momentum of the event, p_t missing, the most energetic μ transverse momentum and the most energetic b-quark transverse momentum, for the “only b-tag” sample. The distributions correspond to $\tan\beta = 40$ and $m_{h^0} = 100$ GeV [30].

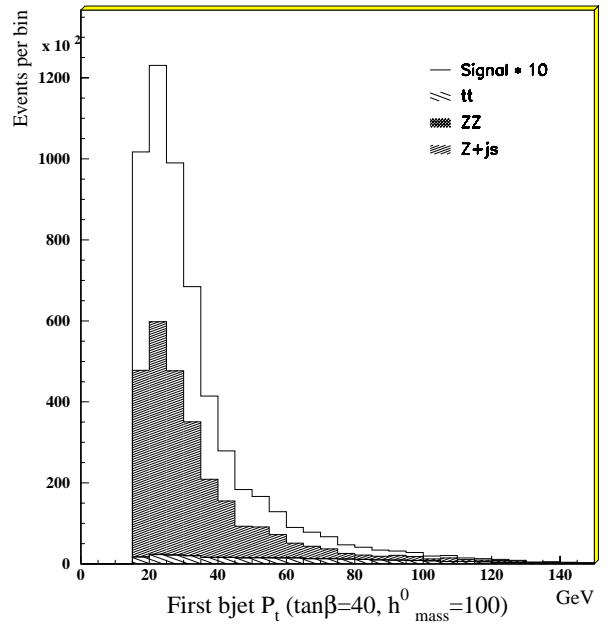
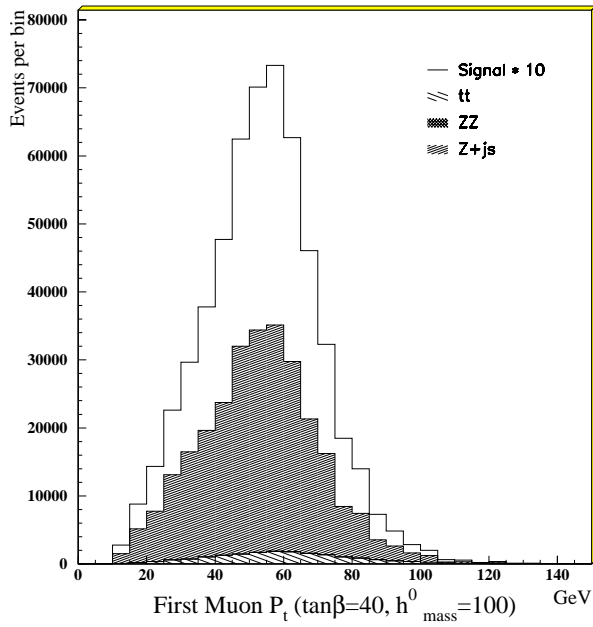
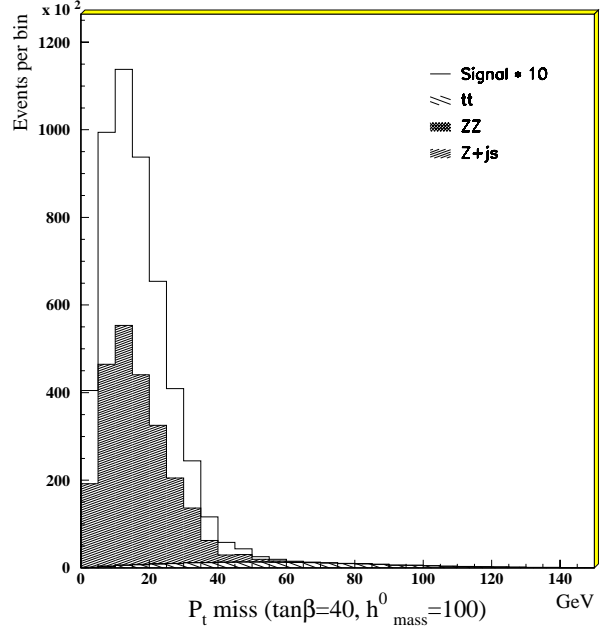
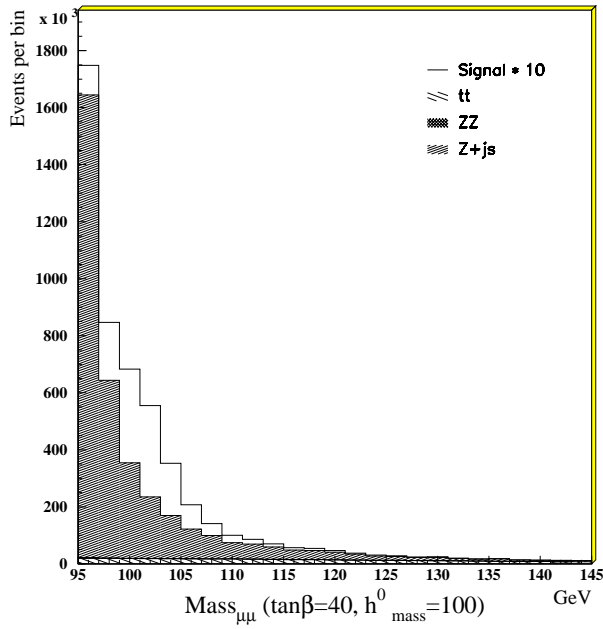


Figure 14: Distributions of the μ -pair invariant mass, of the total transverse missing momentum of the event, p_t missing, the most energetic μ transverse momentum and the most energetic b-quark transverse momentum, for the “only one b-tag” sample. The distributions correspond to $\tan\beta = 40$ and $m_{h^0} = 100$ GeV [30].

At least one b-tag sample, 100 GeV, $\tan\beta = 40$				
	$N_{h\rightarrow\mu\mu}$ $\cdot 10^{-3}$	$N_{t\bar{t}}$ $\cdot 10^{-4}$	N_{ZZ} $\cdot 10^{-3}$	N_{z+jets} $\cdot 10^{-4}$
N_{gen}	328	854	174	$241 \cdot 10^3$
presel.	49	513	62	1621
$P_T^{\mu 1}$	41	364	47	1339
$P_T^{\mu 2}$	32	199	34	1024
$M_{\mu^+\mu^-}$	16.2	9.7	1.0	30
P_T^{b1}	14.8	5.4	0.8	28
P_T^{b2}	12.8	2.2	0.6	25
P_T^{miss}	12.8	1.7	0.6	25

Table 12: Single tag b-tag sample (see text). (see Tab. 11). The number are given for $m_h = 100$ GeV and $\tan\beta = 40$.

The most effective criteria on reduction of $t\bar{t}$ background, as seen in Tab. 11, Tab. 12, Tab. 13 and are those applied on P_T either of b-jets or μ . The $t\bar{t}$ background is also reduced with requiring an upper bound to the P_T missing in the event. Such events are characterized by a large P_T missing due to the presence of neutrinos.

From the tables and the figures the samples of single tag and only one tag appear to have similar characteristics. No other straightforward conclusion can be drawn at such a level.

7 Background subtraction

From the previous discussion it is clear that one of the main difficulties in the h boson search and on the undoubtedly proof of its existence is the precise background knowledge. Nevertheless, this goal has serious difficulties due to the uncertainties on the calculated cross sections, in particularly of the $Z \rightarrow \mu^+\mu^-$ background, and consequently on a *a priory* evaluation with Monte Carlo techniques of the corresponding number of events in the selected sample. In this paragraph a method based on the experimental data is proposed, in principle avoiding all theoretical uncertainties.

The proposed method is based on the experimental data with a final state characterized from two electrons and to b-jets. This final state is exactly as our golden channel, where the two μ of final state are replaced from two electrons. This final state is signal-free due to the depressed branching ratio of neutral h in electrons respect to heavier particles (*e.g.* $\left(\frac{m_\mu}{m_e}\right)^2$). Then, this

Only one b-tag sample, 100 GeV, $\tan\beta = 40$				
	$N_{h\rightarrow\mu\mu}$ $\cdot 10^{-3}$	$N_{t\bar{t}}$ $\cdot 10^{-4}$	N_{ZZ} $\cdot 10^{-3}$	N_{z+jets} $\cdot 10^{-4}$
N_{gen}	328	854	174	$241 \cdot 10^3$
presel.	45	445	50	1541
$P_T^{\mu 1}$	38	314	38	1273
$P_T^{\mu 2}$	30	171	27	974
$M_{\mu^+\mu^-}$	15	8.3	0.8	29
P_T^{b1}	14	4.9	0.6	26
P_T^{b2}	12	2.1	0.5	24
P_T^{miss}	12	1.6	0.5	24

Table 13: Only one b-tag sample (see text) (see Tab. 11). The number are given for $m_h = 100$ GeV and $\tan\beta=40$.

final state is mainly originated from Z decays in electrons. This channel due to the universality of lepton coupling has the same branching ratio of the Z decays in muons. It is consequently well tailored to be used for the evaluation of the background, because the same number of events is expected in the two channels.

Unfortunately this method can't be applied straight forward, for the different response of the detector to final state electron respect muons and for the different *bremhstrahlung* characteristics. This implies that the numbers of select e^+e^- events have to be corrected for different acceptance and resolution of the calorimeter and muon spectrometer and for the different emission of photons.

This effect, the *inner bremhstrahlung* [33], is the emission of a photon near the Ze^+e^- or $Z\mu^+\mu^-$ vertex. The presence of such photon is distorting differently the invariant mass reconstructed, $M_{e^+e^-}$, $M_{\mu^+\mu^-}$. The invariant mass of e^+e^- and $\mu^+\mu^-$ from Z decays are reported in Fig. 15 (on the top) for a sample of 10^7 generated events of both channels. In the Fig. 15 (bottom) of the two invariant mass is shown corrected by photon *bremhstrahlung*.

To take in account this effect the *inner bremhstrahlung* photons with a transverse momentum greater than 7 GeV or in an angular cone of $\Delta R = 0.07$ around the track of one of the two electrons are considered belonging to the electron. This implies that to the four-momentum of the nearest electron the four momentum of the photon is summed up. In Fig. 15 (on the bottom, right) the $M_{e^+e^-}$ is shown taking in account the four momentum of photon *bremhstrahlung*. The difference due to the *inner bremhstrahlung* is reduced to few percent spread. More precisely the spread of the ratio between the

distribution of invariant mass of the $\mu^+\mu^-$ and e^+e^- is reduced from 40% to less than 5% implying less important corrections factors. This effect doesn't affect the continuous background of $t\bar{t}$, which in this subtraction procedure is automatically taken in account.

Another method has been suggested [1] for the background evaluation fitting the distribution of an b-untagged event sample. The two methods rely on different control sample and are affected from different systematics. Both method can be used to have a better check and understanding of background.

8 Results

In the previous paragraphs we have developed the analysis for a set of given points in $(\tan\beta, m_A)$ plane. In this final paragraph, full use of this analysis is made in a complete scan over $(\tan\beta, m_A)$, in the maximal mixing scenario for the Minimal Supersymmetric Standard Model boson h. This results described in this paragraph are obtained with the fast simulation ATLASFAST the complete simulation is not considered. The curve representing the ratio of signal events, S, and background events, B, $S/B = 1\%$ and $S/B = 2\%$ are reported in Fig. 16.

Regions in the discovery potential in ATLAS experiment are shown in Fig. 17 and Fig. 18 corresponding to $\frac{s}{\sqrt{B}} = 5$ and $\frac{s}{\sqrt{B}} = 3$ respectively.

The promising region corresponding to high $\tan\beta \sim 15$ and $m_h \approx 100$ GeV, not excluded from LEP and Tevatron data, is accessible to a possible discovery at LHC.

9 Conclusions

The possibility of MSSM h discovery in region of high $\tan\beta$, larger than 15 and mass close to 100 GeV has been investigated exploiting the decay of neutral h boson in two muons, $h \rightarrow \mu^+\mu^-$, accompanied from two b-jets. This region is not accessible to the others h decay and only to few others MSSM Higgs decay.

The results described in this paper show a well defined possibility for the discovery of a neutral Higgs boson in region traditionally difficult due to the presence of Z resonance. The $\mu^+\mu^-$ decays exploit the high resolution performance of ATLAS detector, the muon spectrometer and the inner detector, together the high b-tagging capability.

A full experimental method to subtract the highest contributing background due to Z boson decay, $Z \rightarrow \mu^+\mu^-$, is suggested. This method rely

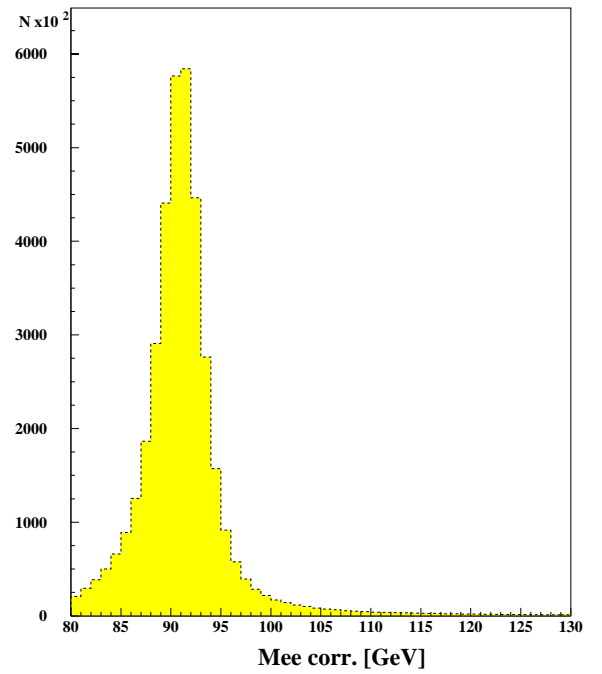
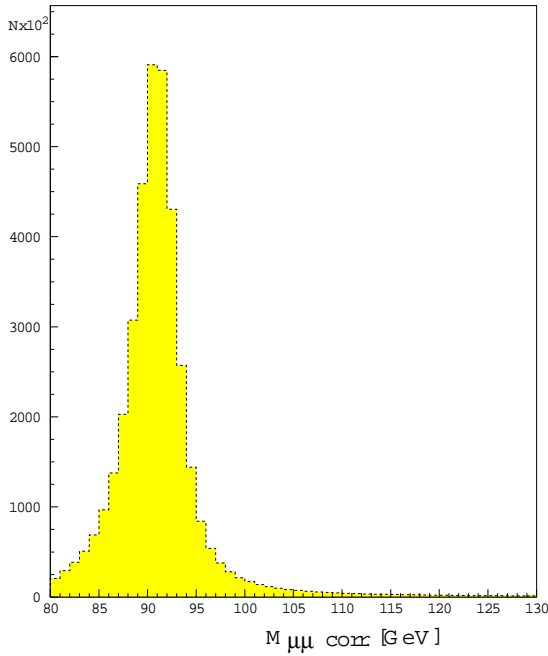
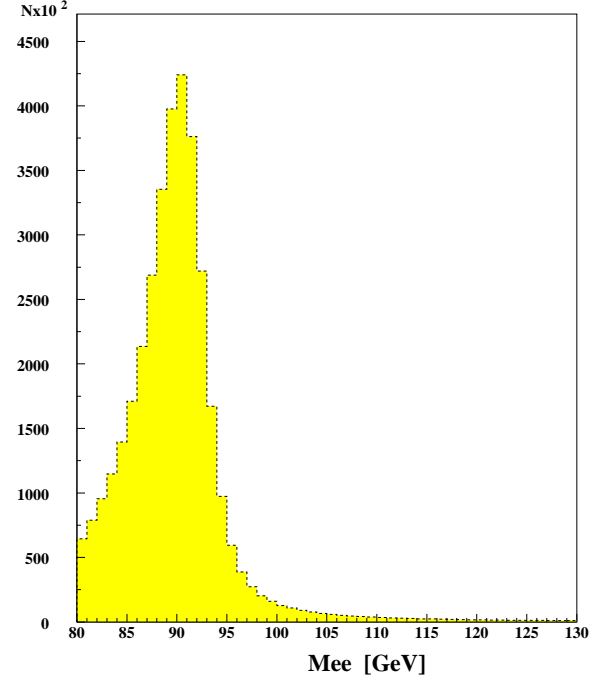
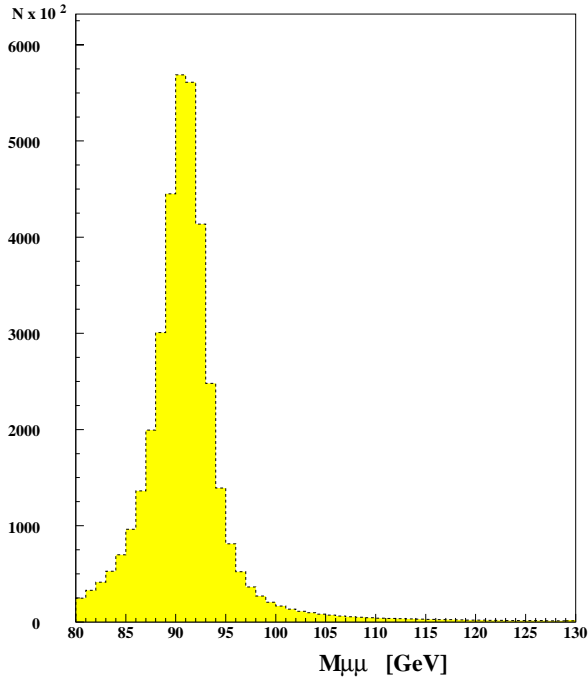


Figure 15:
 Distributions of invariant mass $M_{\mu^+\mu^-}$, $M_{e^+e^-}$ (top). The same quantities $M_{\mu^+\mu^-}$, $M_{e^+e^-}$ after including corrections for bremsstrahlung photons(bottom).

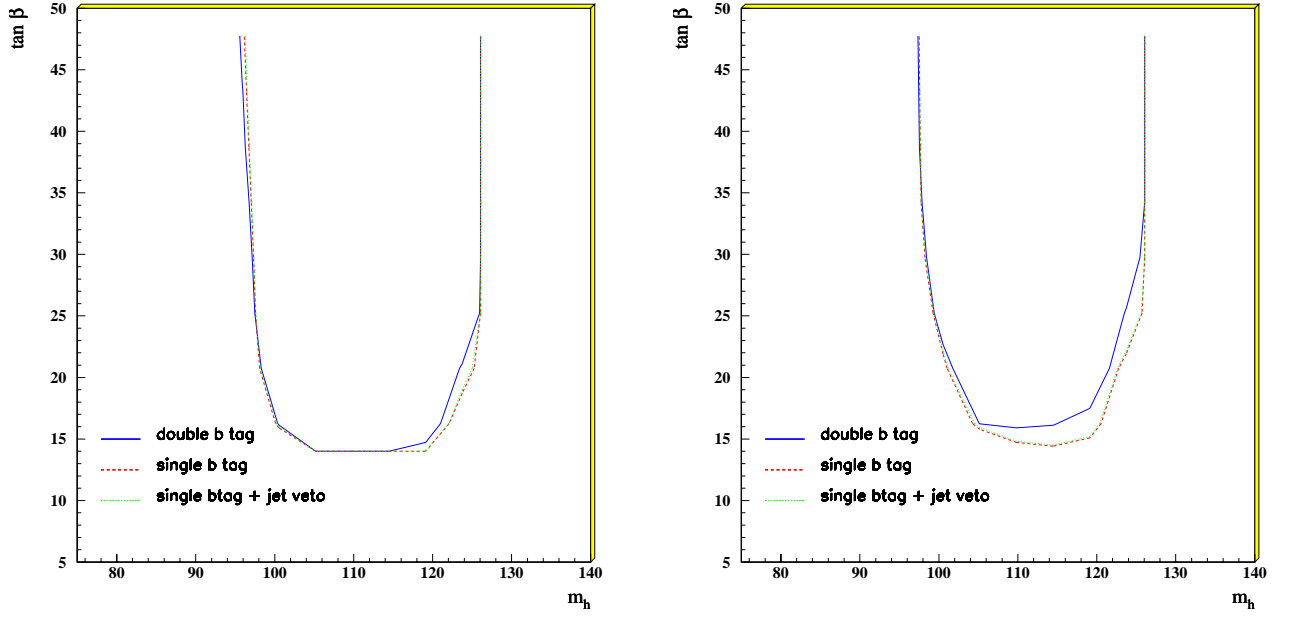


Figure 16: Curves of a constant signal, S to background, B ratio for the neutral MSSM Higgs boson $h \rightarrow \mu^+ \mu^-$ in maximal mixing scenario. The inner curve corresponds to double b-tag sample, indicated as double b tag, the outer curves correspond to at least one b-tag sample, indicated as single b tag, and only one b-tag sample, indicated as single btag +jet veto. The plot on the left is drawn for signal to background ratio, $\frac{S}{B} = 0.01$ and on the right for $\frac{S}{B} = 0.02$. The integrated corresponding luminosity is $\int \mathcal{L} dt = 300 \text{ fb}^{-1}$.

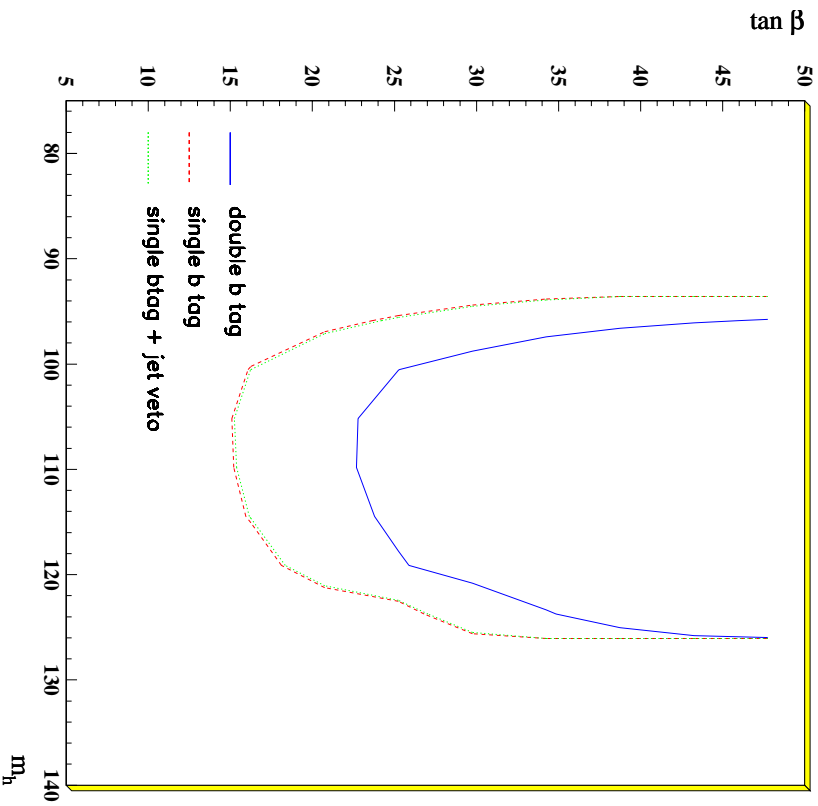


Figure 17: Plot of discovery potential for neutral MSSM Higgs boson $b \rightarrow \mu^+ \mu^-$ and two b-jets in maximal mixing scenario. The inner curve corresponds to double b-tag sample, indicated as double b tag, the outers curve correspond to at least one b-tag, indicated as single b tag, and only one b-tag, indicated as single btag +jet veto. The plot is drawn for signal significance $\frac{s}{\sqrt{B}} = 5$. The integrated corresponding luminosity is $\int \mathcal{L} dt = 300 \text{ fb}^{-1}$.

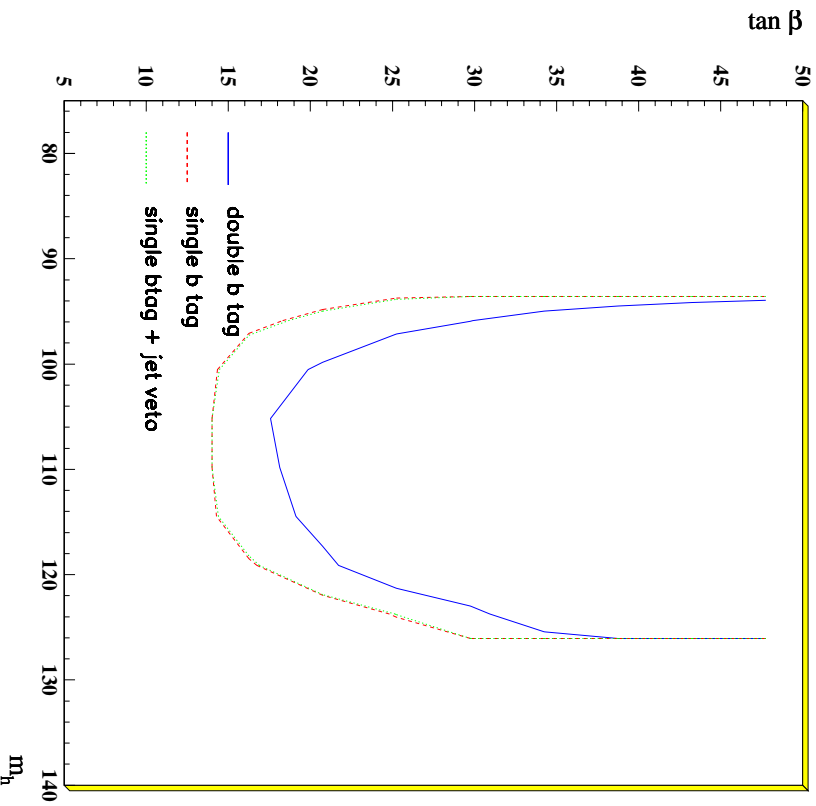


Figure 18: Plot of discovery potential for neutral MSSM Higgs boson $b \rightarrow \mu^+ \mu^-$ and two b-jets in maximal mixing scenario. The inner curve corresponds to double b-tag sample, indicated as double b tag, the outers curve correspond to at least one b-tag, indicated as single b tag, and only one b-tag, indicated as single btag +jet veto. The plot is drawn for signal significance, $\frac{s}{\sqrt{B}} = 3$. The integrated corresponding luminosity is $\int \mathcal{L} dt = 300 \text{ fb}^{-1}$.

mainly on experimental data, with limited Monte Carlo corrections. This procedure is based on the use of a control sample of Z boson decay in electrons, $Z \rightarrow e^+e^-$. The lepton universality guarantees the same numbers of events produced in the Z decays in electrons as well in muons. This simple method is not depending neither from the complex theoretical calculations neither from their implementation in Monte Carlo.

10 Acknowledgments

We wish to thank Prof.Elzbieta Richter-Was for the helpful discussion and constructive criticism. We gratefully acknowledge the help given from Dr. Pavel Nevski and Dr.Jean-Francois Laporte in the software. We also want thank Prof. Guido Ciapetti for the support given to this work.

References

- [1] S. Gonzales, E.Ros, M. Vos, IFIC, University of Valencia/CSIC, Spain: IFIC-PHYS-2002, ATL-PHYS-2002-021, 2002.
- [2] H.-P. Nilles, Phys. Rep. (1984) 1.
- [3] H. E. Haber and G. L. Kane, Phys. Rep. (1985) 75.
- [4] R. Barbieri, Riv. Nuovo Cim. (1988) 11.
- [5] The ALEPH and DELPHI and L3 and and OPAL Collaborations and the LEP Higgs working group, LHWG Note 2002-01 (2002).
- [6] The ALEPH and DELPHI and L3 and and OPAL Collaborations and the LEP Higgs working group, LHWG Note 2001-04 (2001).
- [7] The ALEPH and DELPHI and L3 and and OPAL Collaborations and the LEP Higgs working group, LHWG Note 2001-04 (2001).
- [8] S. Martin, “A supersymmetry primer ”, Kane,G.L. ed.; HEP-PH/9709356 (1999).
- [9] M. Peskin, “Beyond Standard Model ”, SLAC-PUB7479; HEP-PH/9705479 (1997); Lectures given in The 1996 European School of High Energy Physics, Carry-Le-Rouet 1996.
- [10] J.F. Gunion *et al.*, in The Higgs Hunter’s Guide, (Addison Wesley, 1990), p. 191.
- [11] Particle Data Group, D.E.Groom *et al.*, EPJ (2000) 1.
- [12] M. Carena, M.Quiros, C. Wagner, Nucl.Phys. (1996) 407.
- [13] H. Haber, R. Hempfling, A. Hoang, Z.Phys. (1997) 539.
- [14] S. Heinemeyer,W. Hollik, G.Weiglein, Phys. Lett. (1999) 179.
- [15] R.J. Zhang, Phys. Lett. (1999) 89.
- [16] J. R. Espinosa, R.J. Zhang, JHEP (2000) 26.
- [17] A.Brignole, G. Degrassi, P.Slavich,F. Zwirner, Nucl.Phys (2002) 195.

- [18] M.Carena *et al.*, Suggestions of Improved Benchmark Scenarios for Higgs-Boson searches at LEP2:
report CERN-TH/99-374(1999), DESY 99-186, hep-ph/9912223.
- [19] ALEPH Collaboration, A. Heister *et al.*, Phys. Lett. **B 526** (2002) 191.
- [20] DELPHI Collaboration, J. Abdallah *et al.*, Eur. Phys. J. **C 23** (2002) 409.
- [21] L3 Collaboration, M. Acciarri *et al.*, Phys. Lett. **B 545** (2002) 30.
- [22] OPAL Collaboration, G. Abbiendi *et al.*, Eur. Phys. J. **C 12** (2000) 567.
- [23] CMS Coll., Technical Proposal, report CERN/LHCC/94-38 (1994).
- [24] ATLAS Coll., ATLAS Detector and Physics Performance:
Technical Design Report, Volume 2, report CERN/LHCC/99-15 (1999).
- [25] D.Cavalli *et al.*, HEP-PH/020356 (2002).
- [26] E.Richter-Was *et al.*, J. Mod. Phys. (1998) 1371.
- [27] Fabiola Gianotti, Presentation at LHC Committee 5 July 2003.
- [28] ATLAS Coll., Muon Spectrometer Technical Design Report:
Technical Design Report, report CERN/LHCC/97-2 (1997).
- [29] ATLAS Coll., Inner Detector Technical Design Report:
Technical Design Report, report CERN/LHCC/97-17 (1997).
- [30] (1993), revised August 1995; Comp. Phys. Comm. **82** (1994) 74;
Preprint hep-ph/0001032 (2000).
- [31] Mercedes Paniccia, Ricerca del bosone di Higgs nei modelli supersimmetrici al Large Hadron Collider con l'esperimento ATLAS.
tesi di laurea, Universit la Sapienza, Roma, January 2003.
- [32] E.Richter-Was *et al.*: Atlfast 2.0, a package for fast simulation. ATLAS Internal Note, ATL-PHYS-08-031.
- [33] O.Linossier and L. Poggioli, Final state inner-bremsstrahlung effects on $h \rightarrow ZZ^* \rightarrow \ell^+ \ell^- \ell^+ \ell^-$ channel with ATLAS, ATLAS Internal Note, ATL-PHYS-95-075 (1995).